Inorganic Chemistry

Article

pubs.acs.org/IC

Influence of Rotator Design on the Speed of Self-Assembled Four-Component Nanorotors: Coordinative Versus Dispersive Interactions

Pronay Kumar Biswas,[†] Suchismita Saha,[†] Yerramsetti Nanaji, Anup Rana, and Michael Schmittel*

Center of Micro- and Nanochemistry and Engineering, University of Siegen, Adolf−Reichwein−Str. 2, D-57068 Siegen, Germany

Supporting Information

ABSTRACT: Four-component nanorotors are prepared by the self-assembly of stator $[Cu_4(\mathbf{4})]^{4+}$ with its four copper(I)-loaded phenanthroline stations and various rotators carrying one, two, or three pyridine terminals. The fourth component, 1,4-diazabicyclo[2.2.2]octane, serves as a connecting axle between rotator and stator. Capitalizing on the heteroleptic pyridyl and phenanthroline metal complexes concept, the rotator's pyridine terminals are connected to the copper(I)-loaded phenanthroline stations ($N_{py} \rightarrow [Cu(phen)]^+$) in the STOP state and disconnected in the transition state of rotation. As the barrier of the thermally activated rotation, measured by variable-temperature ^1H NMR, is mainly governed by attractive forces between stator stations and rotator terminals, it increases along the series E_a (monopyridine rotator) < E_a (dipyridine rotator) < E_a (tripyridine rotator). However, there are even distinct differences in rate between rotors with equal number of rotator terminals. The change from the 5,10-dipyridyl (*cis*) to 5,15-dipyridyl (*trans*) zinc porphyrin rotator enhances the rotational frequency by almost 1000-fold. Density functional theory computational results suggest that not only coordinative $N_{py} \rightarrow [Cu(phen)]^+$ interactions but also dispersive attraction influence the barrier of rotation.

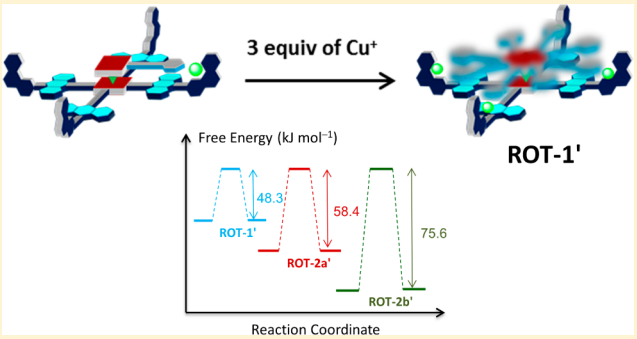

INTRODUCTION

The mode of operation of many biological motors[1] is based on a stepwise rotary motion, as, for instance, in adenosine 5′-diphosphate (ATP) synthase[2,3] driving the synthesis of ATP from adenosine 5′-triphosphate (ADP). Being inspired from the gamut of rotary motions in living cells, chemists have been designing increasingly complex artificial molecular machines.[4−7] Among them, unidirectional molecular motors,[8−11] gears,[12,13] pumps,[14] walkers,[15−17] caterpillars,[18] etc. have gained ample interest. However, most advanced machineries are assembled in a covalent fashion until now, whereas biological machines like the ATP synthase are typically composed of various components. Artificial multicomponent machineries remain extremely rare, because the tools for the spatiotemporal heteroassembly are still limited.[19] Notable exceptions have been reported by Stoddart[20] (supramolecular elevator) and by Shionoya,[21,22] Shinkei,[23] Kume/Nishihara,[24,25] Kobayashi,[26] Crowley,[27] Takeuchi,[28] as well as our group[29,30] (supramolecular nanorotors). Currently, structural variations in artificial multicomponent machinery and their effects on the kinetics of motion remain largely unexplored, because most designs do not tolerate decisive spatiotemporal changes. Any improvement of the working efficiency of molecular machinery, however, will require the optimization of static and moving parts, as in real-world machines.

Our design of supramolecular nanorotors[29] comprises four distinct components: (a) stator, (b) rotator, and two connectors, that is, (c) metal ion(s) and (d) a hinge. Additionally, speed regulation in such multicomponent nanorotors was demonstrated by addition of external brake stones as a fifth component.[29,31] In the present work, we will describe the influence of the rotator design on the speed of the nanorotor and the unexpected finding of the importance of dispersive interactions[32−34] in the rate-determining step.

RESULTS AND DISCUSSION

In the above-mentioned multicomponent supramolecular nanorotors,[29,30] two differently decorated zinc porphyrins (stator and rotator) are sandwiched together by means of two axial $N_{DABCO} \rightarrow$ zinc(II) porphyrin (ZnPor)[35] and two $N_{py} \rightarrow [Cu(phen)]^+$ interactions (DABCO = 1,4-diazabicyclo[2.2.2]octane; phen = phenanthroline; py = pyridine), a construction principle that we will also use in the present study (see Figure 1). The $N_{py} \rightarrow [Cu(phen)]^+$ interaction connects the pyridine terminals (N_{py}) of the rotator with the copper(I)-loaded phenanthroline stations $[Cu(phen)]^+$ of the stator via the HETeroleptic PYridine and Phenanthroline (HETPYP) complexation strategy,[36,37] which involves complexes of type $[Cu(phen)(py)]^+$. Because the copper(I) ion is surrounded by only three strong donors, such complexes are less stable and more dynamic than those of the

Received: March 25, 2017

DOI: 10.1021/acs.inorgchem.7b00740
Inorg. Chem. XXXX, XXX, XXX−XXX

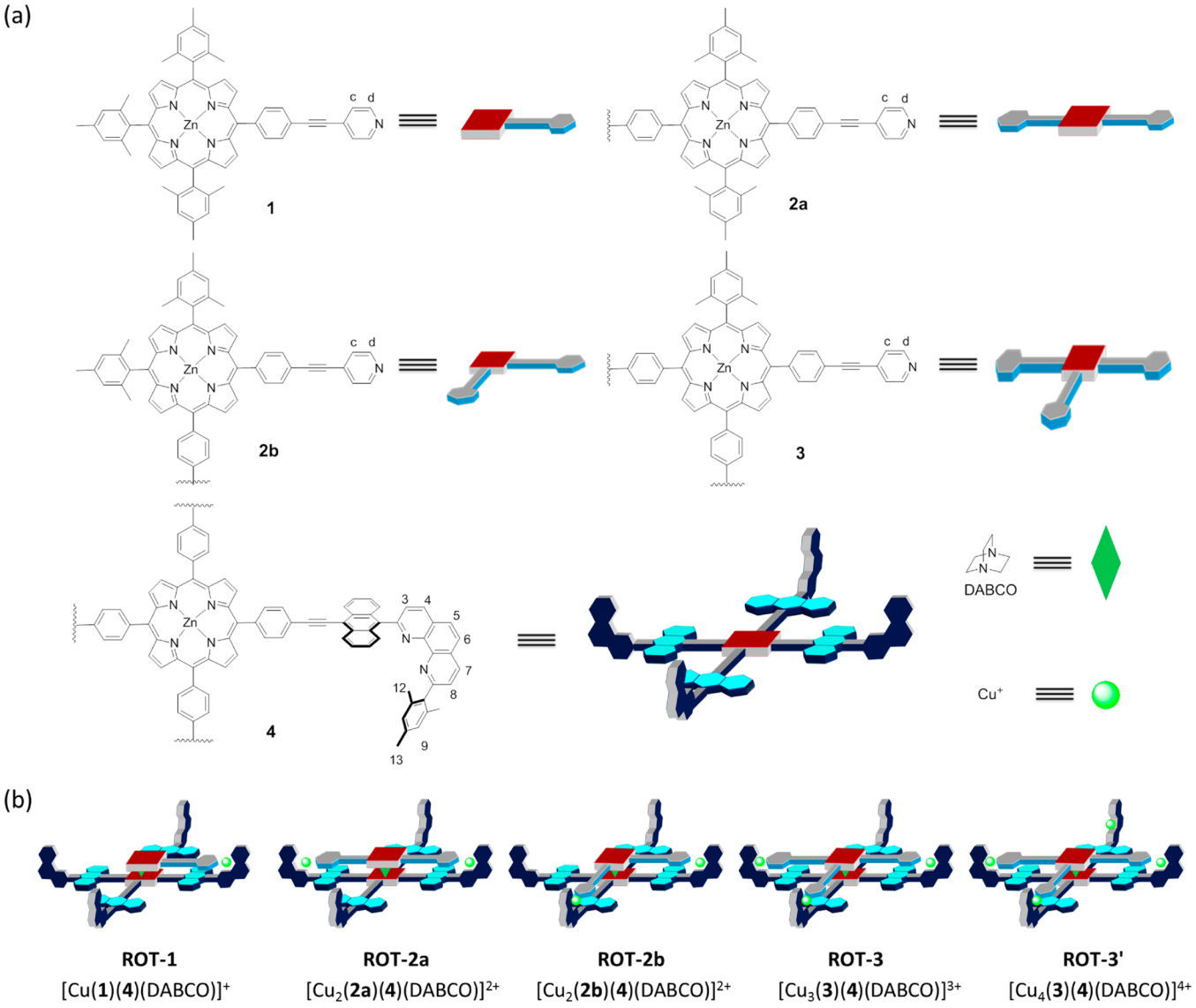

Figure 1. (a) All four components of the self-assembled nanorotors and their cartoon representations. (b) Cartoon representations of the four-component nanorotors.

type $[Cu(phen)_2]^+$. It is thus no surprise that, by our rotor design, the rotator moves with respect to the stator about DABCO as a dynamic hinge by cleaving the $N_{py} \rightarrow [Cu(phen)]^+$ interaction(s).[29]

To quantitatively afford HETPYP complexes of type $[Cu(phen)(py)]^+$, the copper(I) phenanthroline motifs in the stator must be sterically shielded, since thereby competitive formation of the thermodynamically more stable homoleptic copper phenanthroline complexes $[Cu(phen)_2]^+$ is prevented.[38−40] In contrast, steric shielding does not preclude the construction of HETPYP complexes. Their formation is driven by coordinative interactions ($N_{py} \rightarrow [Cu(phen)]^+$) and by $\pi-\pi$ stacking between the pyridine and the aryl moieties of the shielded phenanthroline. To get some further insight into the rotational speed and its dependency on the rotator's nature, structurally different rotators with a varying number of pyridine terminals along with possible isomers (**1**, **2a**, **2b**, **3**) were investigated (Figure 1).

To evaluate the $N_{py} \rightarrow [Cu(phen)]^+$ interaction separately, 1 equiv of $[Cu(CH_3CN)_4]PF_6$ was mixed with 1 equiv of ligand **5** (Figure 2), the latter representing the shielded phenanthroline station in the stator. The reaction furnished exclusively **C1** = $[Cu(\mathbf{5})]^+$, as seen in the ^{1}H NMR from protons 9-H, 3,8-H, 4,7-H, and 5,6-H of **5** that are all shifted downfield due to the electron-demanding metal ion (Figure 2b). Then, 1 equiv of 4-iodopyridine (**6**) was added to **C1**. The resulting heteroleptic complex **C2** = $[Cu(\mathbf{5})(\mathbf{6})]^+$ was characterized unambiguously by ^{1}H NMR, ^{1}H−^{1}H COSY, and electrospray ionization mass spectrometry (ESI-MS). In the ^{1}H NMR spectrum, proton 9-H (Figure 2b) and all anthracene protons experience an upfield shift owing to the shielding effect of the pyridine ring (Supporting Information, Figure S39). Reciprocally, the pyridine protons c-H and d-H are shifted upfield from 7.69 and 8.69 ppm to 7.25 and 6.54 ppm, respectively, because of the shielding effect of both the anthracene and mesityl moieties (Figure 2b). They appear as broad signals due to the dynamic nature of **C2**. From a UV−vis titration the binding constant of **6** to **C1** = $[Cu(\mathbf{5})]^+$ in CH_2Cl_2 was determined as log K = 3.6 ± 0.1 (Supporting Information, Figure S90). To study experimentally the dynamics, ligands **5**, **6** and $[Cu(CH_3CN)_4]$-PF_6 were mixed in 2:1:2 ratio to furnish a 1:1 mixture of **C1** and **C2**. At room temperature, the ^{1}H NMR of the **C1**/**C2**

DOI: 10.1021/acs.inorgchem.7b00740
Inorg. Chem. XXXX, XXX, XXX−XXX

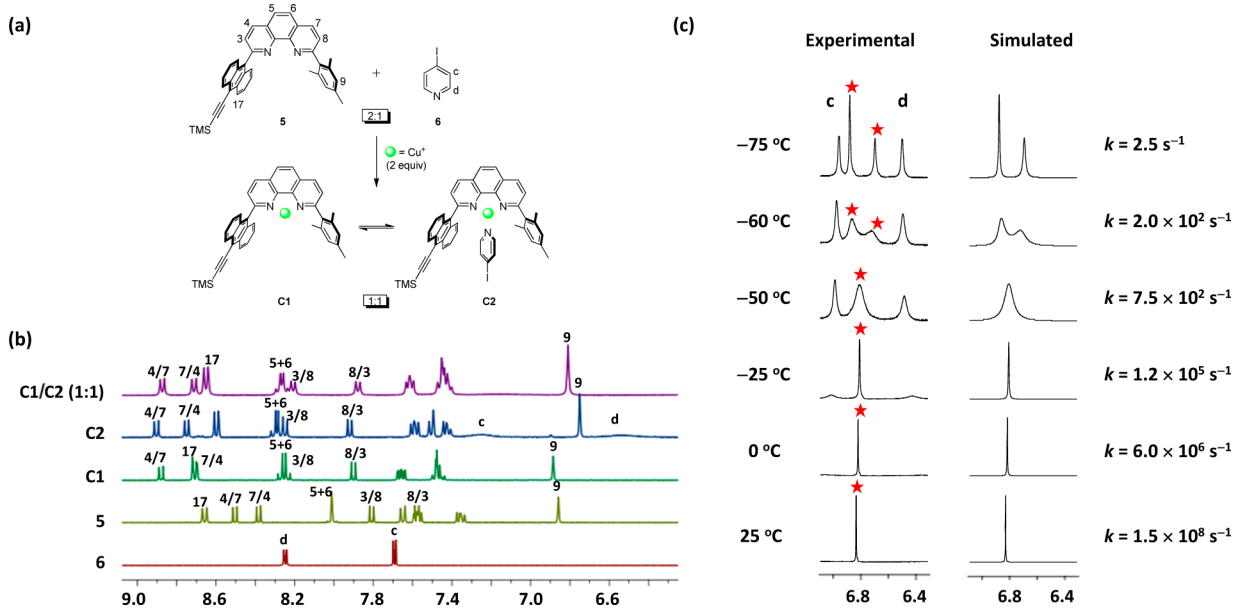

Figure 2. (a) Model complexes **C1** and **C2**. (b) Comparison of partial ^{1}H NMR (CD_2Cl_2, 400 MHz, 298 K) of **6**, **5**, **C1**, **C2** and **C1**/**C2** (1:1). (c) Partial VT ^{1}H NMR (CD_2Cl_2, 600 MHz) of **C1**/**C2** showing the splitting of 9-H (asterisk marked).

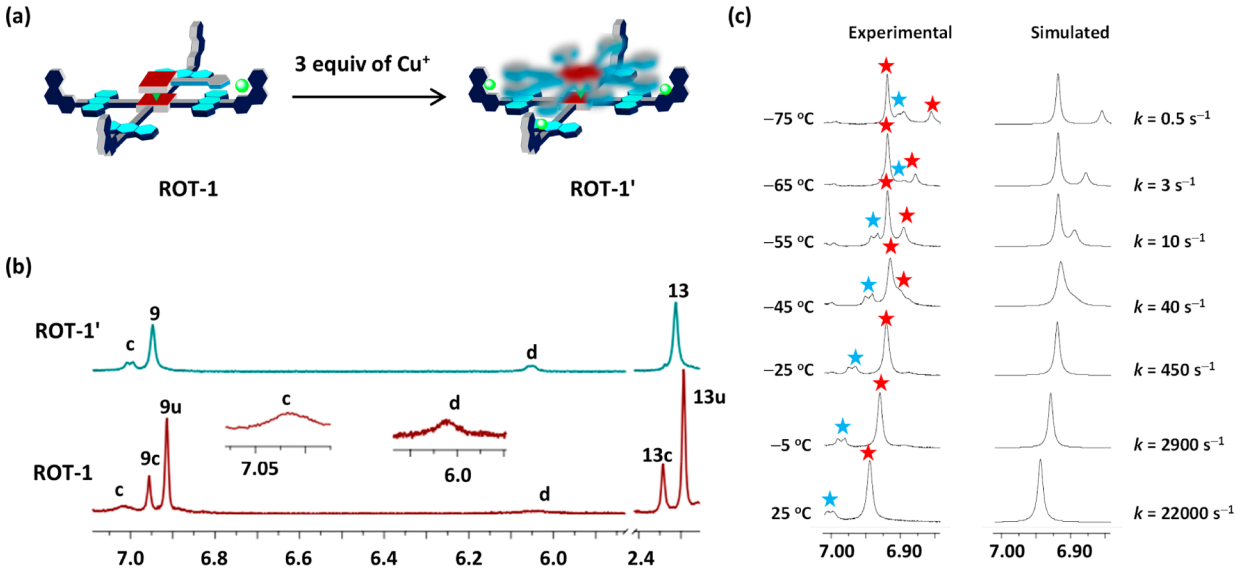

Figure 3. (a) Cartoon representation of **ROT-1** and **ROT-1′**. (b) Comparison of partial ^{1}H NMR (CD_2Cl_2, 400 MHz, 298 K) of **ROT-1** and **ROT-1′**. Protons that correspond to the HETPYP-complexed phenanthroline (9c-H, 13c-H) are different from those that belong to the unloaded phenanthrolines (9u-H, 13u-H) and the averaged signals (9-H and 13-H) in **ROT-1′**. (c) Partial VT ^{1}H NMR (CD_2Cl_2, 600 MHz) of **ROT-1′** shows the splitting of the 9-H signal (red asterisk) and upfield shift of c-H upon lowering temperature (blue asterisk).

mixture displays a single set of all phenanthroline protons at the average positions of those in **C1** and **C2** (Figure 2b). Because of the very fast dynamic exchange protons c-H and d-H broaden and are impossible to detect in the NMR at room temperature, while they show up at low temperature (Figure 2c). In a variable-temperature (VT) ^{1}H NMR experiment, the signal for protons 9-H splits into two singlets (1:1 ratio: one sharp and one broad) upon lowering the temperature to −75 °C with the coalescence point being at ca. −50 °C (Figure 2c). The two singlets refer to protons 9-H in **C1** (δ = 6.87 ppm) and in **C2** (δ = 6.64 ppm). The exchange rate of pyridine **6** between **C1** and **C2** was determined as ∼150 MHz at 25 °C, which furnishes an activation barrier $\Delta G^{\ddagger}_{298}$ = 26.5 kJ mol^{-1}. As the cleavage of **C2** → **C1** + **6** is endergonic by $\Delta G_{298} \approx$ 20.5 kJ mol^{-1} (log K = 3.6), the intrinsic barrier of this self-exchange is strongly (77%) determined by the thermodynamics of the pyridine−copper bond cleavage.

The fast dynamics of this self-exchange encouraged us to design a four-component supramolecular nanorotor based on the very same N_{py} → [Cu(**5**)]$^+$ coordination motif. Therefore, rotators **1**, **2a**, **2b**, and **3** were synthesized by Sonogashira coupling of the corresponding zinc(II)-(4-iodophenyl)-mesitylporphyrins with 4-ethynylpyridine. Details are given in the Supporting Information. To prepare **ROT-1** (Figure 1), rotator **1** was mixed with stator **4**, DABCO, and [Cu-$(CH_3CN)_4$]PF_6 (1:1:1:1) in CD_2Cl_2. As anticipated, the NMR displays two singlets (3:1 ratio) for mesityl protons 9-H at 6.92 and 6.96 ppm (Figure 3b). The pyridine protons d-H

DOI: 10.1021/acs.inorgchem.7b00740
Inorg. Chem. XXXX, XXX, XXX−XXX

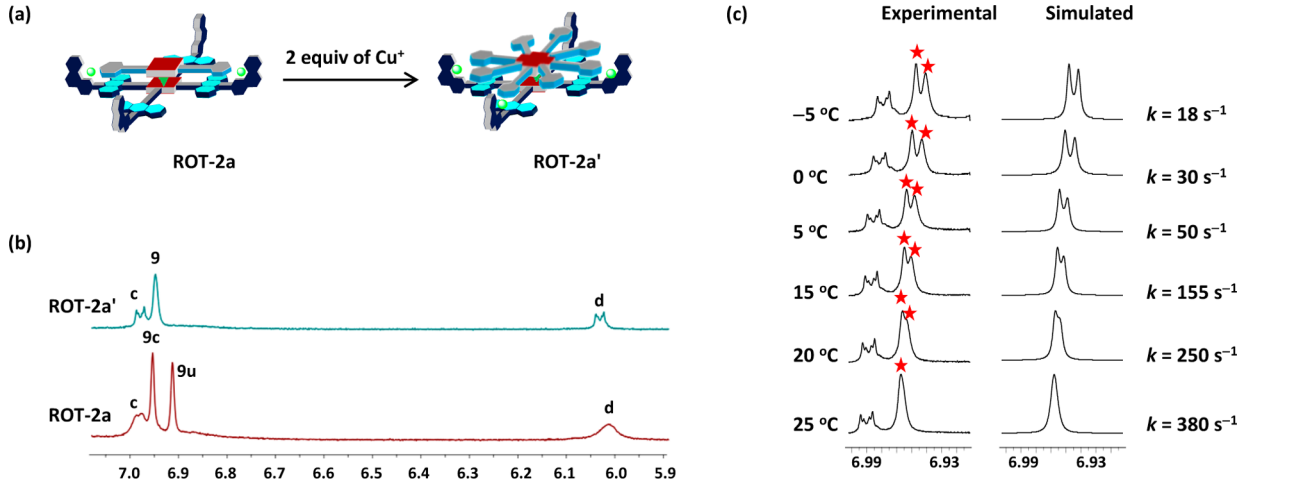

Figure 4. (a) Cartoon representation of **ROT-2a** and **ROT-2a′**. (b) Comparison of partial ^{1}H NMR (CD_2Cl_2, 400 MHz, 298 K) of **ROT-2a** and **ROT-2a′**. Mesityl protons 9c-H and 9u-H denote protons at C-9 of HETPYP-complexed and unloaded phenanthrolines, respectively, in **ROT-2a**. Alike, 9-H represents the averaged proton signal in **ROT-2a′**. (c) Partial VT ^{1}H NMR (CD_2Cl_2, 600 MHz) of **ROT-2a′** showing the splitting of 9-H signal (red asterisk). The signal downfield to 9-H refers to c-H.

and c-H are dynamically broadened and exhibit a diagnostic upfield shift to 6.02 and 7.02 ppm, respectively, due to the shielding effects of the mesityl and anthracenyl groups of **4**. Two sets of broad singlets at −4.57 and −4.85 ppm corresponding to the DABCO protons confirm that DABCO acts as hinge between the two different zinc porphyrins **1** and **4** (Supporting Information, Figure S40).[29,31]

All phenanthroline protons (3-H, 4-H, 5-H, 6-H, 7-H, and 8-H) show as two sets of signals at a 3:1 ratio as well. One of the signal sets is shifted more downfield than the other: the former refers to the HETPYP-complexed phenanthroline protons, while the upfield-shifted set of signals belongs to the uncoordinated phenanthroline stations. The ^{1}H NMR shifts thus clearly confirm formation of **ROT-1** as a heterosandwich structure, which was additionally characterized by ^{1}H−^{1}H COSY, ESI-MS, and elemental analysis. The finding of separate sets of protons (3:1) seems to advocate that **ROT-1** is a static assembly. However, fact is that there is no observable present for detecting the motion (= cleavage and reassociation of the rotator arm at the single copper phenanthroline station). After addition of 3 equiv more of $[Cu(CH_3CN)_4]PF_6$ to **ROT-1**, the resulting **ROT-1′** (Figure 3a) shows fully averaged signals for protons 9-H and 13-H (Figure 3b) as well as for all other phenanthroline station protons (Supporting Information, Figure S42). ^{1}H-DOSY corroborates that **ROT-1′** is a single species in solution (Supporting Information, Figure S70). In **ROT-1′** 16 equiv of CH_3CN (arising from four $[Cu(CH_3CN)_4]PF_6$) stabilize the copper(I) phenanthroline complex units that are not coordinated to the rotator arm. Without CH_3CN, the rotor assembly is unstable, most likely because the $[Cu(phen)]^+$ station is not stable as such without contact to the pyridine arm but may be stabilized as $[Cu(phen)\ (CH_3CN)_n]^+$ (n = 1 or 2).

The dynamic spinning in the nanorotor was monitored by VT ^{1}H NMR in the range from 25 to −75 °C in CD_2Cl_2 (Figure 3c). At 25 °C, protons 9-H appear as a sharp singlet at 6.95 ppm, while upon lowering the temperature the singlet starts to broaden at ca. −45 °C. Below this temperature, a splitting of the singlet peak into two sets of singlets was observed. Upon lowering the temperature further, the separation between the two singlets increases, and at −75 °C the two singlets appear at 6.85 and 6.92 ppm (1:3). These two singlets are assigned to Cu^+-loaded phenanthroline stations that are either connected to the pyridine terminal or not. The characteristic upfield shift of the pyridine protons c-H upon lowering the temperature may be explained owing to the increasing $\pi-\pi$ stacking from the aryl groups of the phenanthroline stations (Figure 3c). These findings suggest that at 25 °C all four phenanthroline stations behave chemically equivalent due to rotation in **ROT-1′**. While the VT ^{1}H NMR provides the rate constant k = 22 000 s^{-1} at 25 °C, the rotation is almost frozen (k = 0.5 s^{-1}) at −75 °C. The free energy activation barrier for exchange in **ROT-1′** is 48.3 kJ mol^{-1} at 25 °C, which is much higher than that in the model system (cf. $\Delta G^{\ddagger}_{298}$ = 26.5 kJ mol^{-1}). As a consequence, the $N_{py} \rightarrow [Cu(\mathbf{5})]^+$ bond cleavage is much more difficult in **ROT-1′** than in the model system (k_{rel} = 1:6800). Several effects may contribute to this difference: (i) in the rotor cooperative stabilization is possible, (ii) in case of the model complex **C2** there are several departure pathways possible to cleave the $N_{py} \rightarrow [Cu(\mathbf{5})]^+$ bond that are prevented in **ROT-1′**, and (iii) significant dispersive attractions present in **ROT-1′** arising from surface contact between stator and rotator additionally contribute to the reduced speed of **ROT-1′** (vide infra).

In the following, the rotors were varied by implementing the dipyridine rotators **2a** (*trans*) and **2b** (*cis*) and the tripyridine rotator **3**. In all rotors (**ROT-2a′**, **ROT-2b′**, **ROT-3′**, prepared in the same manner as **ROT-1′**) the DABCO protons and protons c-H and d-H show at comparable ^{1}H NMR positions confirming the formation of a bis-porphyrin heterosandwich assembly of stator and rotator (see Supporting Information).

For both dipyridine rotators **2a** and **2b**, one would expect that the pyridine terminals need to depart from phenanthroline stations either simultaneously or stepwise. In both scenarios, the overall transition-state barrier of rotation should be higher than that in **ROT-1′**.

In the ^{1}H NMR spectrum of **ROT-2a′** (*trans*) at 25 °C, mesityl protons 9-H of all four phenanthroline stations appear as a singlet at 6.95 ppm suggesting rapid rotation (Figure 4b). The VT ^{1}H NMR study was performed from 25 to −5 °C at an interval of 5 °C (Figure 4c) showing a splitting of proton 9-H into two singlets (ratio 1:1) with coalescence broadening

DOI: 10.1021/acs.inorgchem.7b00740
Inorg. Chem. XXXX, XXX, XXX−XXX

around 20 °C. The singlets at 6.93 and 6.94 ppm are well-resolved at −5 °C and are assigned to protons 9c-H (for HETPYP complexed) and 9Cu-H (for the Cu^+-loaded phenanthroline stations), respectively. From a simulation of the VT ^{1}H NMR signals, the rate constants were determined between −5 and 25 °C. The rate constant is k = 380 s^{-1} at 25 °C, and the corresponding free energy activation barrier is 58.4 kJ mol^{-1}.

In the ^{1}H NMR of **ROT-2b′**, received after addition of 2 equiv of $[Cu(CH_3CN)_4]PF_6$ to **ROT-2b**, protons 9c-H and 9Cu-H do not form an averaged signal. Since they remain separated, there is either no or very slow rotation on the NMR time scale. In such scenarios, the ^{1}H−^{1}H ROESY experiment is a very valuable tool to detect any slow exchange between two separated signals (k_{ex} = 0.2−100 Hz).[18,41] If the rotor is spinning in this frequency range, HETPYP-complexed phenanthroline moieties should exhibit exchange correlation signals with the Cu^+-loaded phenanthroline moieties. Indeed, all proton signals of the HETPYP-complexed phenanthroline stations show exchange correlation in the ^{1}H−^{1}H ROESY with Cu^+-loaded phenanthroline stations. The well-separated protons 12-H signals were chosen to calculate the rate of rotation (Figure 5c). The signals indicate slow exchange at a rate constant k = 0.4 s^{-1} (25 °C).

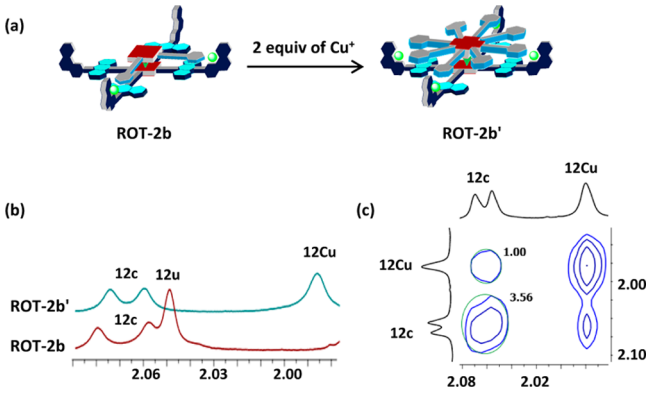

Figure 5. (a) Cartoon representation of **ROT-2b** and **ROT-2b′**. (b) Comparison of partial ^{1}H NMR (CD_2Cl_2, 400 MHz, 298 K) of **ROT-2b** and **ROT-2b′**. Protons 12c-H, 12u-H, and 12Cu-H correspond to 12-H of HETPYP-complexed phenanthroline, unloaded phenanthroline, and Cu^+-loaded phenanthroline, respectively. (c) Partial ^{1}H−^{1}H ROESY NMR (CD_2Cl_2, 600 MHz, 298 K) of **ROT-2b′**.

From earlier discussions regarding rotary motion it is expected that in the case of **ROT-3′** due to presence of three arms, the kinetic stabilization will be even higher than that of **ROT-2a′** or **ROT-2b′**. As a consequence, rotation of **ROT-3′** should be very slow. Indeed, the ^{1}H NMR of **ROT-3′** shows that phenanthroline protons 9-H (9c-H and 9Cu-H) remain separated as in case of **ROT-2b′**. In the ^{1}H−^{1}H ROESY study, none of the protons for HETPYP-complexed and the Cu^+-loaded phenanthroline stations show any kind of exchange correlation (Supporting Information, Figure S68), which clearly suggests that **ROT-3′** just behaves as a nondynamic hetero bis-porphyrin sandwich assembly (k < 0.1 Hz at 25 °C).

From the discussion of all the rotors it is clear that the rotational speed follows the trend **ROT-1′** > **ROT-2a′** > **ROT-2b′** > **ROT-3′**, while the corresponding free energy barriers follow the reverse (Table 1).

Table 1. Experimental Rotational Frequency and Activation Barriers at 25 °C, Calculated from VT ^{1}H NMR

model/ nanorotor	$\Delta H^{\ddagger}$ (kJ mol^{-1})	$\Delta S^{\ddagger}$ (J mol^{-1} K^{-1})	$\Delta G^{\ddagger}_{25}$ (kJ mol^{-1})	k_{25} (s^{-1})
C1/C2 (1:1)			26.5	1.5×10^8
ROT-1′	49.7	6.3	48.3	2.2×10^4
ROT-2a′	66.5	28.1	58.4	3.8×10^2
ROT-2b′			75.6	0.4
ROT-3′			>79.0	<0.1

By comparing the rotator's structure in different rotors, one would expect $\Delta G^{\ddagger}$ values for **ROT-2a′** and **ROT-2b′** to be qualitatively double than that of **ROT-1′** due to presence of doubled binding sites. Surprisingly, $\Delta G^{\ddagger}$ values for both **ROT-2a′** and **ROT-2b′** are much less than double than that of **ROT-1′**. A classic interpretation would be that the binding in both **ROT-2a′** and **ROT-2b′** is accompanied by significant strain that is fully released in the transition state (in Figure 6,

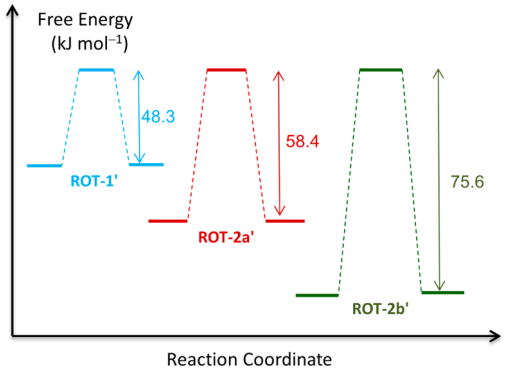

Figure 6. Experimentally determined free energies of activation for the nanorotors in this study, setting the transition states to the same energy level.

transition states are set to the same energy level). Among both rotors, $\Delta G^{\ddagger}$ for **ROT-2a′** deviates even more from the expected value (2 × 48.3 = 96.6 kJ mol^{-1}). To comprehend the reasons behind it, we took a closer view at both rotors, expecting that the $\Delta\Delta G^{\ddagger}$ may primarily be the consequence of two factors: either (a) ground-state or (b) transition-state differences.

Clearly, the rotary motion is faster in case of **ROT-2a′** (k = 380 s^{-1}) than in **ROT-2b′** (k = 0.4 s^{-1}), albeit both rotators have similar binding sites that differ only in spatial orientation. For further clarification we decided to investigate the energy profile of the rotation computationally. To speed the computations while using a relatively large basis set, the simple model system (**ROT-4**, Figure 7) was constructed. In **ROT-4**, both the rotator and stator are monoarm compounds with hydrogens at the *meso*-positions of the porphyrins. First, we optimized **ROT-4** at B3LYP-D3(BJ)-gCP/def2-SVP level. To obtain computational transition state (TS) energies close to the experimental data, one acetonitrile (CH_3CN) had to be coordinated to the copper(I) ion of **ROT-4**, while another one had to be added for nucleophilic displacement of the rotator arm. In our search for the TS we increased the distance between the copper and pyridine nitrogen (Cu^1−N^2). When the Cu^1−N^2 bond distance increased in **ROT-4** (Figure 7), the Cu^1−N^3 bond distance (between copper and the attacking acetonitrile) started to decrease automatically. The results suggest a TS with a barrier height of 33.9 kJ mol^{-1} for the

DOI: 10.1021/acs.inorgchem.7b00740
Inorg. Chem. XXXX, XXX, XXX−XXX

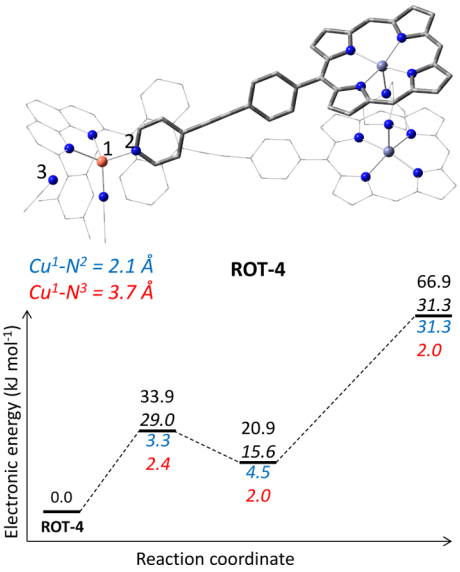

Figure 7. Energy profile of rotary motion of **ROT-4**. The black numbers are relative electronic energies (B3LYP-D3(BJ)-gCP/def2-SVP), while the corresponding italics give relative energies after inclusion of solvation (B3LYP-D3(BJ)-gCP/def2-SVP/COSMO-(CH_2Cl_2)//B3LYP-D3(BJ)-gCP/def2-SVP). The colored numbers provide the bond distances.

breaking of HETPYP binding. Surprisingly though, when the rotator and stator arm were constrained opposite to each other (at a dihedral angle of 180°, no binding possible), the energy of the system is much higher (66.9 kJ mol^{-1}) than that of the TS (33.9 kJ mol^{-1}). Thus, the Cu^1–N^2 bond breaking only contributes roughly half to the full barrier. The other portion of the barrier arises from the loss of attractive interactions between stator and rotator arms. The corresponding dispersive attractions develop all the way from the zinc porphyrin until the binding sites of stator and rotator. Because the barrier height of 66.9 kJ mol^{-1} (gas phase) is much too high compared to the experimental number (48.3 kJ mol^{-1}), a solvent correction[42] was implemented, which indeed brought down the computed barrier to 31.3 kJ mol^{-1} (at B3LYP-D3(BJ)-gCP/def2-SVP/COSMO(CH_2Cl_2)//B3LYP-D3(BJ)-gCP/def2-SVP level).

Three different "conformational" states can be realized in **ROT-2a′** and **ROT-2b′**. In **State-1** (Figure 8), none of the rotator arms is coordinated to copper(I) centers. At the same time, there is no surface contact between rotator and stator arms. In contrast, in **State-2**, both rotator arms are coordinated to copper(I) centers as illustrated in Figure 8. **State-3** can be realized as a mixture of **State-1** and **State-2**; that is, one rotator arm is coordinated to the copper(I) phenanthroline station, and the other one is lying on top of the adjacent stator arm without contact to the copper(I) center. Because computations on **ROT-4** support **State-1** as the TS for rotation, the **States-2** and **3** are possible starting minima.

Computations at B3LYP-D3(BJ)/3-21G level predict that both rotators **2a** and **2b** are of similar energy (ΔE = 0.2 kJ mol^{-1}) as free compounds.[43] Because attractive/repulsive forces between stator and rotator arms are not present in **State-1**, rotors **ROT-2a′** and **ROT-2b′** should exhibit identical absolute energies (Figure 9). Thus, the different rotational rates of **ROT-2a′** and **ROT-2b′** should arise from energetic differences in the ground states, that is, either from **State-2** or **State-3**. Surprisingly, computational results at B3LYP-D3(BJ)/3-21G predict that **State-3** is energetically preferred over **State-2** for both rotors. In case of **ROT-2a′**, the former one is preferred by 14.0 kJ mol^{-1}, and for **ROT-2b′** the same preference is 31.3 kJ mol^{-1}. A detailed investigation suggests that these differences arise mainly due to dispersive stabilization of **State-3** for both rotors (see Supporting Information).

After identification of **State-3** as the ground state of the nanorotors, the isodesmic reaction **ROT-2a′**(**State-3**) + **2b** →

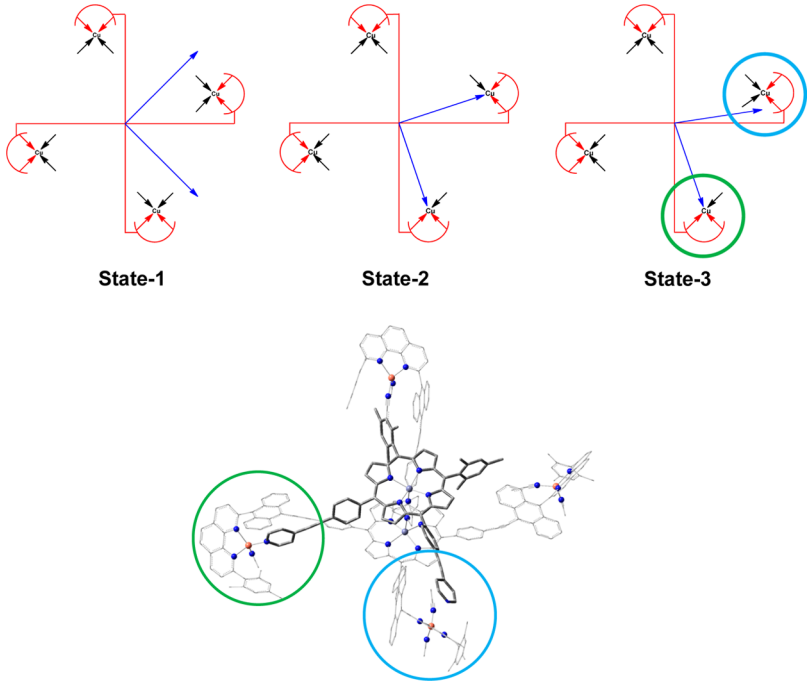

Figure 8. (top) Views of three states for **ROT-2b′** are shown. Similar states for **ROT-2a′** were also considered but not shown in this figure. The red colored portion is for stator, the blue one is for rotator, and the black one is for acetonitrile. (bottom) The figure represents **State-3** of **ROT-2b′**.

DOI: 10.1021/acs.inorgchem.7b00740
Inorg. Chem. XXXX, XXX, XXX−XXX

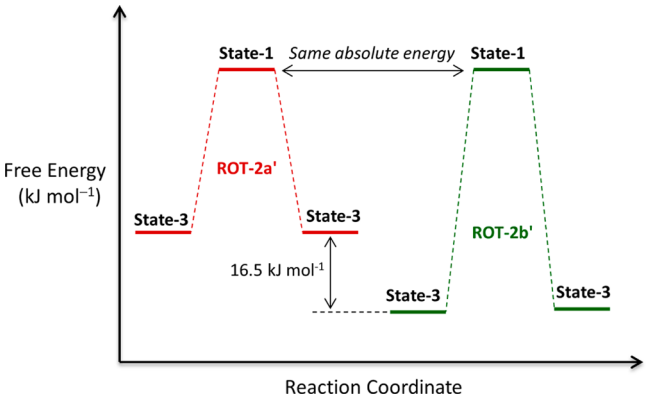

Figure 9. Rotational energy profile for **ROT-2a′** and **ROT-2b′** (computed).

ROT-2b′(State-3) + **2a**, should provide insight in the relative ground-state energies. Accordingly, rotor **ROT-2b′** has a lower ground-state energy than **ROT-2a′**, by 16.5 kJ mol^{-1}! This energy difference matches very well with the experimentally observed barrier difference of 17.2 kJ mol^{-1} at 25 °C suggesting that the different kinetics of **ROT-2a′** and **ROT-2b′** arises exclusively from different ground-state energies. The origin of the differential ground-state stabilization can be best rationalized by differences in dispersive attraction. **ROT-2b′** receives 28.0 kJ mol^{-1} more stabilization from dispersion than **ROT-2a′**.

On the one hand, in **ROT-1′** with its single-arm rotator **1** the single HETPYP linkage and the rather small dispersive stabilization between rotator and stator lead to maximum speed. On the other hand, in **ROT-3′** with its three-arm rotator (**3**), three HETPYP linkages and strong dispersive stabilization prevent any rotation at room temperature.

CONCLUSION

In conclusion, we demonstrate that our approach to supramolecular four-component nanomachinery allows variation of rotator without compromising on the basis function of a thermally activated nanorotor.[10] As predicted, strong binding between the departing pyridine terminals and the copper phenanthroline stations controls the rotational speed of the machinery. Importantly, this binding involves both coordinative (N_{py} → [Cu(phen)]$^+$) and attractive dispersive interactions. On increasing the number of binding interactions, the activation barrier for the rotation increases. In case of the triarm rotator, the rotation stops completely. On moving from the *trans* to *cis* diarm rotor, that is, changing only the spatial orientation of the binding sites, the rotational speed of the nanorotor is reduced by a factor of ca. 1000. Computational results suggest that this drastic change is due to dispersive attractions[31−33] stabilizing the ground state of the *cis* rotor. The variation of rotational speed by structural change of the rotator suggests further investigations on the role of other rotor's components on the overall function and speed.

EXPERIMENTAL SECTION

Bruker Avance (400 MHz) and Varian (600 MHz) spectrometers were used to measure ^{1}H and ^{13}C NMR spectra using a deuterated solvent as the lock and residual protiated solvent as internal reference ($CDCl_3$: δ_H 7.26 ppm, δ_C 77.0 ppm; CD_2Cl_2: δ_H 5.32 ppm, δ_C 53.8 ppm, tetrahydrofuran-d_8: δ_H 1.72 ppm, 3.58 ppm, δ_C 25.3 ppm, 67.2 ppm). The following abbreviations were used to define NMR peak patterns: s = singlet, d = doublet, t = triplet, dd = doublet of doublets, ddd = doublet of doublets of doublets, bs = broad singlet, m = multiplet. The coupling constant values are given in hertz (Hz). Full proton assignments are given in Supporting Information. Electrospray ionization (ESI-MS) spectra were recorded on a Thermo-Quest LCQ deca. Melting points of compounds were measured on a BÜCHI 510 instrument and are not corrected. Infrared spectra were recorded on a Varian 1000 FT-IR instrument. Elemental analysis was performed using the EA-3000 CHNS analyzer. UV−vis spectra were recorded on a Cary Win 50 (298 K) spectrometer.

Pre-Rotor Complex ROT-1. In an NMR tube, stator **4** (1.65 mg, 0.619 μmol) was mixed with 1 equiv of $[Cu(CH_3CN)_4]PF_6$ (0.234 mg, 0.619 μmol) salt and dissolved in a small amount of CD_2Cl_2, followed by addition of rotator **1** (0.560 mg, 0.619 μmol) and DABCO (69.0 μg, 0.619 μmol). After subsequent sonication for 10 min the complex was obtained in quantitative yield. **mp**: decomp > 60 °C. **IR** (KBr): ν = 3442, 3435, 3066, 3037, 2952, 2924, 2851, 2336, 2218, 1620, 1601, 1487, 1444, 1380, 1203, 1097, 995, 848, 796, 767, 641, 629, 558 cm^{-1}. **^{1}H NMR** (CD_2Cl_2, 400 MHz): δ = −4.85 (bs, 6H), −4.57 (bs, 6H), 1.26 (s, 9H), 1.54 (s, 9H, f′-H), 1.97 (s, CH_3, CH_3CN from $[Cu(CH_3CN)_4]PF_6$), 2.05 (s, 18H), 2.06 (s, 6H), 2.29 (s, 9H), 2.34 (s, 3H), 2.60 (s, 9H), 6.02 (bs, 2H), 6.92 (s, 6H), 6.96 (s, 2H), 7.02 (bs, 2H), 7.26 (bs, 6H), 7.47−7.57 (m, 10H), 7.63 (d, ^3J = 8.2 Hz, 3H), 7.66 (d, ^3J = 8.2 Hz, 2H), 7.73−7.81 (m, 18H), 7.89 (bs, 2H), 7.94 (d, ^3J = 8.2 Hz, 3H), 8.02 (d, ^3J = 8.2 Hz, 1H), 8.06 (d, ^3J = 8.8 Hz, 3H), 8.08 (d, ^3J = 8.8 Hz, 3H), 8.16−8.22 (m, 8H), 8.31−8.37 (m, 11H), 8.41 (d, ^3J = 4.2 Hz, 2H), 8.43 (d, ^3J = 8.2 Hz, 3H), 8.53 (d, ^3J = 4.2 Hz, 2H), 8.59 (d, ^3J = 8.2 Hz, 3H), 8.73 (s, 4H), 8.76 (d, ^3J = 4.6 Hz, 2H), 8.78 (d, ^3J = 4.6 Hz, 2H), 8.82 (d, ^3J = 8.2 Hz, 1H), 8.96 (d, ^3J = 8.8 Hz, 2H), 9.02 (d, ^3J = 8.2 Hz, 1H), 9.04 (d, ^3J = 8.8 Hz, 6H) ppm. Anal. Calcd for $C_{258}H_{185}CuF_6N_{19}PZn_2{\cdot}9CH_2Cl_2$: C, 69.19; H, 4.50; N, 6.01. Found: C, 68.89; H, 4.40; N, 5.72%. **ESI-MS**: *m*/*z* (%) 1816.8 (100) $[Cu(\mathbf{1})(\mathbf{4}){\cdot}H]^{2+}$.

Nanorotor ROT-1′. $[Cu(CH_3CN)_4]PF_6$ (3 equiv, 0.692 mg, 1.86 μmol) was added to **ROT-1**. After sonication for 10 min **ROT-1′** formed quantitatively. **mp**: decomp > 60 °C. **IR** (KBr): ν = 3445, 2952, 2923, 2853, 2221, 1654, 1616, 1491, 1442, 1382, 1202, 995, 855, 850, 767, 560 cm^{-1}. **^{1}H NMR** (CD_2Cl_2, 400 MHz): δ = −4.80 (bs, 6H), −4.60 (bs, 6H), 1.26 (s, 9H), 1.36 (s, 6H), 1.65 (s, 3H), 1.97 (s, CH_3, CH_3CN from $[Cu(CH_3CN)_4]PF_6$), 2.01 (s, 24H), 2.31 (s, 12H), 2.60 (s, 3H), 2.61 (s, 6H), 6.05 (d, ^3J = 5.6 Hz, 2H), 6.95 (s, 8H), 7.00 (d, ^3J = 5.6 Hz, 2H), 7.05 (bs, 2H), 7.17 (s, 3H), 7.40 (s, 3H), 7.57−7.65 (m, 16H), 7.78−7.83 (m, 12H), 7.96 (d, ^3J = 8.2 Hz, 6H), 8.22 (bs, 10H), 8.28−8.36 (m, 18H), 8.41 (d, ^3J = 4.6 Hz, 2H), 8.55 (d, ^3J = 4.6 Hz, 2H), 8.75 (bs, 12H), 8.95 (d, ^3J = 8.2 Hz, 4H), 9.05 (d, ^3J = 8.8 Hz, 8H) ppm. **Elemental analysis**: Upon removal of CH_3CN (which arises from the Cu(I) salt), the assembly is not stable. **ESI-MS**: *m*/*z* (%) 955.8 (100) $[Cu_4(\mathbf{1})(\mathbf{4})]^{4+}$, 730.4 (20) $[Cu_4(\mathbf{4})]^{4+}$.

Pre-Rotor Complex ROT-2a. In an NMR tube, stator **4** (1.48 mg, 0.554 μmol) and 2 equiv of $[Cu(CH_3CN)_4]PF_6$ (0.413 mg, 1.11 μmol) were dissolved in a small amount of CD_2Cl_2, followed by addition of rotator **2a** (0.534 mg, 0.554 μmol) and DABCO (62.1 μg, 0.554 μmol). Subsequent sonication for 10 min furnished the complex in quantitative yield. **mp**: decomp > 60 °C. **IR** (KBr): ν = 3439, 2957, 2923, 2852, 2331, 2221, 1604, 1488, 1450, 1202, 995, 845, 795, 767, 758, 641, 558 cm^{-1}. **^{1}H NMR** (CD_2Cl_2, 400 MHz): δ = −4.85 (bs, 6H), −4.76 (bs, 6H), 1.31 (s, 6H), 1.72 (s, 6H), 1.97 (s, CH_3, CH_3CN from $[Cu(CH_3CN)_4]PF_6$), 2.05 (s, 12H), 2.06 (s, 12H), 2.30 (s, 6H), 2.35 (s, 6H), 2.61 (s, 6H), 6.02 (d, ^3J = 5.6 Hz, 4H), 6.87 (bs, 2H), 6.92 (s, 4H), 6.96 (s, 4H), 6.98 (d, ^3J = 5.6 Hz, 4H), 7.15 (s, 2H), 7.43 (s, 2H), 7.48−7.51 (m, 4H), 7.53−7.57 (m, 6H), 7.63−7.68 (m, 12H), 7.73−7.82 (m, 14H), 7.96 (d, ^3J = 8.0 Hz, 2H), 8.03 (d, ^3J = 8.0 Hz, 2H), 8.06 (d, ^3J = 8.8 Hz, 2H), 8.09 (d, ^3J = 8.8 Hz, 2H), 8.15−8.23 (m, 10H), 8.33−8.39 (m, 8H), 8.43 (bs, 4H), 8.44 (d, ^3J = 8.0 Hz, 2H), 8.57 (bs, 4H), 8.60 (d, ^3J = 8.0 Hz, 2H), 8.75 (d, ^3J = 4.4 Hz, 4H), 8.78 (d, ^3J = 4.4 Hz, 4H), 8.84 (d, ^3J = 8.0 Hz, 2H), 8.95 (d, ^3J = 8.8 Hz, 4H), 8.98 (d, ^3J = 8.0 Hz, 2H), 9.04 (d, ^3J = 8.8 Hz, 4H) ppm. Anal. Calcd for $C_{262}H_{182}Cu_2F_{12}N_{20}P_2Zn_2{\cdot}7CH_2Cl_2$: C, 67.98; H, 4.16; N, 5.89. Found: C, 68.40; H, 4.26; N, 5.61%. **ESI-MS**: *m*/*z* (%) 1877.4 (100) $[Cu_2(\mathbf{2a})(\mathbf{4})]^{2+}$, 1678.9 (45) $[Cu_4(\mathbf{4})\ (DABCO)\ (CH_3CN)]$-

DOI: 10.1021/acs.inorgchem.7b00740
Inorg. Chem. XXXX, XXX, XXX−XXX

$(PF_6)_2^{2+}$, 1629.3 (25) $[Cu_4(\mathbf{4})\ (CH_3CN)](PF_6)_2^{2+}$, 1252.0 (20) $[Cu_2(\mathbf{2a})(\mathbf{4})]^{3+}$, 930.4 (5) $[Cu_2(\mathbf{4})]^{3+}$.

Nanorotor ROT-2a′. $[Cu(CH_3CN)_4]PF_6$ (2 equiv, 0.413 mg, 1.11 μmol) was added to **ROT-2a**. Sonication for 10 min afforded **ROT-2a′** quantitatively. **mp**: decomp > 60 °C. **IR** (KBr): ν = 3444, 2967, 2922, 2851, 2218, 1616, 1489, 1482, 1482, 1439, 1200, 995, 852, 848, 768, 559 cm^{-1}. **^{1}H NMR** (CD_2Cl_2, 400 MHz): δ = −[4.85−4.82] (m, 6H), −[4.77−4.73] (m, 6H), 1.32 (s, 6H), 1.73 (s, 6H), 1.93 (s, CH_3, CH_3CN from $[Cu(CH_3CN)_4]PF_6$), 1.98 (s, 12H), 2.06 (s, 12H), 2.31 (s, 6H), 2.34 (s, 6H), 2.61 (s, 6H), 6.06 (d, ^3J = 5.6 Hz, 4H), 6.87 (bs, 2H), 6.95 (s, 8H), 6.98 (d, ^3J = 5.6 Hz, 4H), 7.14 (s, 2H), 7.42 (s, 2H), 7.53−7.57 (m, 6H), 7.59−7.66 (m, 14H), 7.73−7.80 (m, 6H), 7.84−7.88 (m, 4H), 7.93 (d, ^3J = 8.0 Hz, 2H), 8.02 (d, ^3J = 8.0 Hz, 2H), 8.16 (d, ^3J = 8.0 Hz, 6H), 8.24 (d, ^3J = 8.0 Hz, 6H), 8.27−8.39 (m, 16H), 8.42 (d, ^3J = 4.8, 4H), 8.58 (d, ^3J = 4.8, 4H), 8.72−8.75 (m, 6H), 8.78 (d, ^3J = 4.4, 4H), 8.82 (d, ^3J = 8.0, 2H), 8.93−8,96 (m, 6H), 8.98 (d, ^3J = 8.0, 2H), 9.09 (d, ^3J = 8.8 Hz, 4H) ppm. **Elemental analysis**: Upon removal of CH_3CN (which arises from the Cu(I) salt), the assembly is not stable. **ESI-MS**: *m*/*z* (%) 970.3 (100) $[Cu_4(\mathbf{2a})(\mathbf{4})]^{4+}$.

Pre-Rotor Complex ROT-2b. In an NMR tube, stator **4** (1.16 mg, 0.435 μmol) and 2 equiv of $[Cu(CH_3CN)_4]PF_6$ (0.325 mg, 0.871 μmol) were dissolved in CD_2Cl_2, followed by addition of rotator **2b** (0.420 mg, 0.435 μmol) and DABCO (49.0 μg, 0.435 μmol). Subsequent sonication for 10 min furnished the complex in quantitative yield. **mp**: decomp > 60 °C. **IR** (KBr): ν = 3853, 3441, 2957, 2922, 2852, 2213, 1601, 1487, 1443, 1202, 995, 844, 795, 767, 757, 628, 615, 607, 557 cm^{-1}. **^{1}H NMR** (CD_2Cl_2, 400 MHz): δ = −[4.88−4.85] (m, 6H), −[4.81−4.77] (m, 6H), 1.50 (s, 6H), 1.51 (s, 6H), 1.97 (s, CH_3, CH_3CN from $[Cu(CH_3CN)_4]PF_6$), 2.05 (s, 12H), 2.06 (s, 6H), 2.08 (s, 6H), 2.29 (s, 6H), 2.35 (s, 6H), 2.60 (s, 6H), 6.03 (d, ^3J = 6.4 Hz, 4H), 6.91 (s, 4H), 6.95 (s, 2H), 6.98 (s, 2H), 7.00 (d, ^3J = 6.4 Hz, 4H), 7.04 (d, ^3J = 8.0 Hz, 2H), 7.18 (s, 2H), 7.37 (s, 2H), 7.48−7.52 (m, 4H), 7.54−7.58 (m, 6H), 7.63 (d, ^3J = 8.0 Hz, 2H), 7.64 (d, ^3J = 8.0 Hz, 2H), 7.66−7.70 (m, 4H), 7.74−7.80 (m, 14H), 7.88 (d, ^3J = 8.0 Hz, 2H), 7.95 (d, ^3J = 8.0 Hz, 2H), 8.00 (d, ^3J = 8.0 Hz, 2H), 8.03 (d, ^3J = 8.0 Hz, 2H), 8.06 (d, ^3J = 8.8 Hz, 2H), 8.09 (d, ^3J = 8.8 Hz, 2H), 8.17−8.23 (m, 8H), 8.33−8.39 (m, 10H), 8.44 (d, ^3J = 8.0 Hz, 2H), 8.45 (d, ^3J = 4.4 Hz, 2H), 8.49 (d, ^3J = 8.0 Hz, 2H), 8.54 (d, ^3J = 4.4 Hz, 2H), 8.58−8.60 (m, 4H), 8.71 (s, 2H), 8.75 (d, ^3J = 4.4 Hz, 2H), 8.78 (d, ^3J = 4.4 Hz, 2H), 8.81 (s, 2H), 8.83 (d, ^3J = 8.0 Hz, 2H), 8.95 (d, ^3J = 8.8 Hz, 4H), 8.98 (d, ^3J = 8.0 Hz, 2H), 9.02 (d, ^3J = 8.8 Hz, 4H) ppm. Anal. Calcd for $C_{262}H_{182}Cu_2F_{12}N_{20}P_2Zn_2{\cdot}6CH_2Cl_2$: C, 68.96; H, 4.19; N, 6.00. Found: C, 68.94; H, 4.35; N, 5.65%. **ESI-MS**: *m*/*z* (%) 1877.4 (100) $[Cu_2(\mathbf{2b})(\mathbf{4})]^{2+}$, 1679.8 (20) $[Cu_4(\mathbf{4})\ (DABCO)\ (CH_3CN)](PF_6)_2^{2+}$, 1628.8 (15) $[Cu_4(\mathbf{4})\ (CH_3CN)](PF_6)_2^{2+}$.

Nanorotor ROT-2b′. $[Cu(CH_3CN)_4]PF_6$ (2 equiv, 0.325 mg, 0.871 μmol) was added to **ROT-2b**. Sonication for 10 min afforded **ROT-2b′** quantitatively. **mp**: decomp > 60 °C. **IR** (KBr): ν = 3444, 2964, 2923, 2851, 2218, 1614, 1493, 1442, 1386, 1203, 995, 868, 864, 768, 559 cm^{-1}. **^{1}H NMR** (CD_2Cl_2, 400 MHz): δ = −[4.86−4.82] (m, 6H), −[4.80−4.76] (m, 6H), 1.51 (s, 6H), 1.53 (s, 6H), 1.92 (s, CH_3, CH_3CN from $[Cu(CH_3CN)_4]PF_6$), 1.99 (s, 12H), 2.06 (s, 6H), 2.08 (s, 6H), 2.30 (s, 6H), 2.34 (s, 6H), 2.60 (s, 6H), 6.05 (d, ^3J = 6.4 Hz, 4H), 6.95 (s, 6H), 6.97 (s, 2H), 7.00 (d, ^3J = 6.4 Hz, 4H), 7.05 (d, ^3J = 8.0 Hz, 2H), 7.19 (s, 2H), 7.35 (s, 2H), 7.54−7.63 (m, 12H), 7.66−7.72 (m, 6H), 7.74−7.81 (m, 8H), 7.84−7.90 (m, 6H), 7.94 (d, ^3J = 8.0 Hz, 2H), 8.00 (d, ^3J = 8.0 Hz, 2H), 8.03 (d, ^3J = 8.0 Hz, 2H), 8.14−8.22 (m, 4H), 8.25 (d, ^3J = 8.0 Hz, 4H), 8.28−8.31 (m, 4H), 8.33−8.39 (m, 12H), 8.45 (d, ^3J = 4.4 Hz, 2H), 8.49 (d, ^3J = 8.0 Hz, 2H), 8.55 (d, ^3J = 4.4 Hz, 2H), 8.60 (s, 2H), 8.70 (s, 2H), 8.74 (d, ^3J = 8.0 Hz, 2H), 8.76 (d, ^3J = 4.4 Hz, 2H), 8.80 (d, ^3J = 4.4 Hz, 2H), 8.83 (d, ^3J = 8.0 Hz, 2H), 8.84 (s, 2H), 8.95 (d, ^3J = 8.0 Hz, 2H), 8.96−9.00 (m, 6H), 9.07 (d, ^3J = 8.8 Hz, 4H) ppm. **Elemental analysis**: Upon removal of CH_3CN (which arises from the Cu(I) salt), the assembly is not stable. **ESI-MS**: *m*/*z* (%) 971.5 (100) $[Cu_4(\mathbf{2b})(\mathbf{4})]^{4+}$.

Pre-Rotor Complex ROT-3. In an NMR tube stator **4** (1.31 mg, 0.491 μmol) and 3 equiv of $[Cu(CH_3CN)_4]PF_6$ (0.549 mg, 1.47 μmol) were dissolved in CD_2Cl_2 followed by addition of rotator **3** (0.502 mg, 0.491 μmol) and DABCO (55.0 μg, 0.491 μmol). Subsequent sonication for 10 min furnished the complex in quantitative yield. **mp**: decomp > 60 °C. **IR** (KBr): ν = 2947, 2923, 2852, 2220, 1664, 1608, 1482, 1458, 1379, 1202, 995, 841, 794, 768, 640, 557, 405 cm^{-1}. **^{1}H NMR** (CD_2Cl_2, 400 MHz): δ = −[5.01−4.97] (m, 6H), −[4.94−4.90] (m, 6H), 1.44 (s, 3H), 1.59 (s, 3H, f′-H), 1.97 (s, CH_3, CH_3CN from $[Cu(CH_3CN)_4]PF_6$), 2.06 (s, 6H), 2.07 (s, 9H), 2.08 (s, 9H), 2.30 (s, 3H), 2.35 (s, 9H), 2.61 (s, 3H), 6.01−6.04 (m, 6H), 6.87 (d, ^3J = 8.0 Hz, 2H), 6.92−7.01 (m, 14H), 7.06 (d, ^3J = 8.0 Hz, 2H), 7.18 (s, 1H), 7.39 (s, 1H), 7.49−7.58 (m, 8H), 7.64 (d, ^3J = 8.0 Hz, 1H), 7.65−7.69 (m, 10H), 7.73−7.81 (m, 12H), 7.88 (d, ^3J = 8.0 Hz, 2H), 7.95 (d, ^3J = 8.0 Hz, 1H), 7.99−8.01 (m, 2H), 8.03 (d, ^3J = 8.0 Hz, 3H), 8.08−8.09 (m, 2H), 8.13−8.17 (m, 4H), 8.20−8.24 (m, 4H), 8.33−8.39 (m, 11H), 8.40−8.44, (m, 3H), 8.47 (d, ^3J = 4.4 Hz, 2H), 8.48 (d, ^3J = 8.0 Hz, 2H), 8.57−8.62 (m, 5H), 8.63 (d, ^3J = 4.4 Hz, 2H), 8.73 (d, ^3J = 4.4 Hz, 2H), 8.76 (d, ^3J = 4.4 Hz, 2H), 8.81 (s, 4H), 8.83 (d, ^3J = 8.0 Hz, 3H), 8.93−9.03 (m, 11H) ppm. Anal. Calcd for $C_{266}H_{179}Cu_3F_{18}N_{21}P_3Zn_2{\cdot}7\ CH_2Cl_2$: C, 65.15; H, 3.75; N, 6.08. Found: C, 65.31; H, 3.87; N, 5.86%. **ESI-MS**: *m*/*z* (%) 1329.0 (100) $[Cu_3(\mathbf{3})(\mathbf{4})\ (DABCO)]^{3+}$.

Nanorotor ROT-3′. $[Cu(CH_3CN)_4]PF_6$ (1 equiv, 0.184 mg, 0.491 μmol) was added to **ROT-3**. Subsequent sonication for 10 min afforded **ROT-3′** quantitatively. **mp**: decomp > 60 °C. **IR** (KBr): ν = 2957, 2924, 2853, 2218, 1614, 1384, 1093, 1203, 996, 869, 846, 796, 559 cm^{-1}. **^{1}H NMR** (CD_2Cl_2, 400 MHz): δ = −[5.00−4.96] (m, 6H), −[4.93−4.88] (m, 6H),1.44 (s, 3H), 1.59 (s, 3H), 1.95 (s, CH_3, CH_3CN from $[Cu(CH_3CN)_4]PF_6$), 1.98 (s, 6H), 2.06 (s, 6H), 2.07 (s, 12H), 2.30 (s, 3H), 2.35(s, 9H), 2.60 (s, 3H), 6.02−6.04 (m, 6H), 6.88 (d, ^3J = 8.0 Hz, 2H), 6.95−7.01 (m, 14H), 7.08 (d, ^3J = 8.0 Hz, 2H), 7.18 (s, 1H), 7.37 (s, 1H), 7.53−7.61 (m, 8H), 7.64−7.70 (m, 10H), 7.73−7.79 (m, 10H), 7.84−7.91 (m, 4H), 7.94 (d, ^3J = 8.0 Hz, 1H), 7.99−8.04 (m, 5H), 8.14−8.16 (m, 4H), 8.20−8.26 (m, 4H), 8.26−8.28 (m, 2H), 8.33−8.39 (m, 14H), 8.46−8.48 (m, 4H), 8.57−8.60 (bs, 4H), 8.63 (d, ^3J = 4.4 Hz, 2H) 8.72−8.75 (m, 3H), 8.76 (d, 2H, ^3J = 4.4 Hz), 8.81−8.84 (m, 7H), 8.93−8.99 (m, 10H), 9.07 (d, ^3J = 8.8 Hz, 2H) ppm. **Elemental analysis**: Upon removal of CH_3CN (which arises from the Cu(I) salt), the assembly is not stable. **ESI-MS**: *m*/*z* (%) 985.4 (100) $[Cu_4(\mathbf{3})(\mathbf{4})]^{4+}$.

■ ASSOCIATED CONTENT

Supporting Information

The Supporting Information is available free of charge on the ACS Publications website at DOI: 10.1021/acs.inorgchem.7b00740.

Synthesis and characterization of ligands and model complexes, proton assignment of all rotors, rate constant determination, binding constant measurement, and computational coordinates (PDF)

■ AUTHOR INFORMATION

Corresponding Author

*E-mail: schmittel@chemie.uni-siegen.de.

ORCID

Michael Schmittel: 0000-0001-8622-2883

Author Contributions

†Both authors contributed equally to the paper.

Notes

The authors declare no competing financial interest.

■ ACKNOWLEDGMENTS

We thank the DFG (Schm 647/20-1) and the Univ. of Siegen for continued support, in particular, for providing the Linux Cluster HorUS for computations.

DOI: 10.1021/acs.inorgchem.7b00740
Inorg. Chem. XXXX, XXX, XXX−XXX

REFERENCES

(1) *Molecular Motors;* Schliwa, M., Ed.; Wiley-VCH: Weinheim, Germany, 2002, 582.
(2) Yoshida, M.; Muneyuki, E.; Hisabori, T. ATP synthase - a marvellous rotary engine of the cell. *Nat. Rev. Mol. Cell Biol.* **2001**, *2*, 669−677.
(3) Schliwa, M.; Woehlke, G. Molecular motors. *Nature* **2003**, *422*, 759−765.
(4) Richards, V. 2016 Nobel Prize in Chemistry: Molecular machines. *Nat. Chem.* **2016**, *8*, 1090.
(5) Erbas-Cakmak, S.; Leigh, D. A.; McTernan, C. T.; Nussbaumer, A. L. Artificial Molecular Machines. *Chem. Rev.* **2015**, *115*, 10081−10206.
(6) Astumian, R. D. Artificial Molecular Motors: Running on information. *Nat. Nanotechnol.* **2016**, *11*, 582−583.
(7) Scottwell, S. O.; Crowley, J. D. Ferrocene-containing non-interlocked molecular machines. *Chem. Commun.* **2016**, *52*, 2451−2464.
(8) Browne, W. E.; Feringa, B. L. Making molecular machines work. *Nat. Nanotechnol.* **2006**, *1*, 25−35.
(9) Michl, J.; Sykes, E. C. H. Molecular rotors and motors: recent advances and future challenges. *ACS Nano* **2009**, *3*, 1042−1048.
(10) Ernst, K.-H. Molecular motors: A turn in the right direction. *Nat. Nanotechnol.* **2012**, *8*, 7−8.
(11) Rapenne, G. Synthesis of technomimetic molecules: towards rotation control in single-molecular machines and motors. *Org. Biomol. Chem.* **2005**, *3*, 1165−1169.
(12) Ogi, S.; Ikeda, T.; Wakabayashi, R.; Shinkai, S.; Takeuchi, M. A bevel-gear-shaped rotor bearing a double-decker porphyrin complex. *Chem. - Eur. J.* **2010**, *16*, 8285−8290.
(13) Frantz, D. K.; Linden, A.; Baldridge, K. K.; Siegel, J. S. Molecular spur gears comprising triptycene rotators and bibenzimidazole-based stators. *J. Am. Chem. Soc.* **2012**, *134*, 1528−1535.
(14) Cheng, C.; McGonigal, P. R.; Schneebeli, S. T.; Li, H.; Vermeulen, N. A.; Ke, C.; Stoddart, J. F. An artificial molecular pump. *Nat. Nanotechnol.* **2015**, *10*, 547−553.
(15) von Delius, M.; Geertsema, E. M.; Leigh, D. A. A synthetic small molecule that can walk down a track. *Nat. Chem.* **2010**, *2*, 96−101.
(16) Qu, D.-H.; Tian, H. Synthetic small-molecule walkers at work. *Chem. Sci.* **2013**, *4*, 3031−3035.
(17) Liu, M.; Cheng, J.; Tee, S. R.; Sreelatha, S.; Loh, I. Y.; Wang, Z. Biomimetic Autonomous Enzymatic Nanowalker of High Fuel Efficiency. *ACS Nano* **2016**, *10*, 5882−5890.
(18) Liu, S.; Kondratuk, D. V.; Rousseaux, S. A. L.; Gil-Ramirez, G.; O'Sullivan, M. C.; Cremers, J.; Claridge, T. D. W.; Anderson, H. L. Caterpillar track complexes in template-directed synthesis and correlated molecular motion. *Angew. Chem., Int. Ed.* **2015**, *54*, 5355−5359.
(19) Saha, M. L.; Neogi, S.; Schmittel, M. Dynamic heteroleptic metal-phenanthroline complexes: from structure to function. *Dalton Trans.* **2014**, *43*, 3815−3834.
(20) Badjic, J. D.; Balzani, V.; Credi, A.; Silvi, S.; Stoddart, J. F. A molecular elevator. *Science* **2004**, *303*, 1845−1849.
(21) Hiraoka, S.; Okuno, E.; Tanaka, T.; Shiro, M.; Shionoya, M. Ranging correlated motion (1.5 nm) of two coaxially arranged rotors mediated by helix inversion of a supramolecular transmitter. *J. Am. Chem. Soc.* **2008**, *130*, 9089−9098.
(22) Hiraoka, S.; Hisanaga, Y.; Shiro, M.; Shionoya, M. A molecular double ball bearing: an Ag(I)-Pt(II) dodecanuclear quadruple-decker complex with three rotors. *Angew. Chem., Int. Ed.* **2010**, *49*, 1669−1673.
(23) Ogi, S.; Ikeda, T.; Wakabayashi, R.; Shinkai, S.; Takeuchi, M. A bevel-gear-shaped rotor bearing a double-decker porphyrin complex. *Chem. - Eur. J.* **2010**, *16*, 8285−8290.
(24) Nishikawa, M.; Kume, S.; Nishihara, H. Stimuli-responsive pyrimidine ring rotation in copper complexes for switching their physical properties. *Phys. Chem. Chem. Phys.* **2013**, *15*, 10549−10565.
(25) Takara, Y.; Kusamoto, T.; Masui, T.; Nishikawa, M.; Kume, S.; Nishihara, H. A single-molecular twin rotor: correlated motion of two pyrimidine rings coordinated to copper. *Chem. Commun.* **2015**, *51*, 2896−2898.
(26) Nakamura, M.; Kishimoto, K.; Kobori, Y.; Abe, T.; Yoza, K.; Kobayashi, K. Self-Assembled Molecular Gear: A 4:1 Complex of Rh(III)Cl Tetraarylporphyrin and Tetra(p-pyridyl)cavitand. *J. Am. Chem. Soc.* **2016**, *138*, 12564−12577.
(27) Scottwell, S. Ø.; Elliott, A. B. S.; Shaffer, K. J.; Nafady, A.; McAdam, C. J.; Gordon, K. C.; Crowley, J. D. Chemically and electrochemically induced expansion and contraction of a ferrocene rotor. *Chem. Commun.* **2015**, *51*, 8161−8164.
(28) Shibata, M.; Tanaka, S.; Ikeda, T.; Shinkai, S.; Kaneko, K.; Ogi, S.; Takeuchi, M. Stimuli-Responsive Folding and Unfolding of a Polymer Bearing Multiple Cerium(IV) Bis(porphyrinate) Joints: Mechano-imitation of the Action of a Folding Ruler. *Angew. Chem., Int. Ed.* **2013**, *52*, 397−400.
(29) Samanta, S. K.; Schmittel, M. Four-component supramolecular nanorotors. *J. Am. Chem. Soc.* **2013**, *135*, 18794−18797.
(30) Samanta, S. K.; Bats, J. W.; Schmittel, M. A five-component nanorotor with speed regulation. *Chem. Commun.* **2014**, *50*, 2364−2366.
(31) Samanta, S. K.; Rana, A.; Schmittel, M. Conformational Slippage Determines Rotational Frequency in Five-Component Nanorotors. *Angew. Chem., Int. Ed.* **2016**, *55*, 2267−2272.
(32) Schneider, H.-J. Dispersive interactions in solution complexes. *Acc. Chem. Res.* **2015**, *48*, 1815−1822.
(33) Wagner, J. P.; Schreiner, P. R. London dispersion in molecular chemistry–reconsidering steric effects. *Angew. Chem., Int. Ed.* **2015**, *54*, 12274−12296.
(34) Liptrot, D. J.; Power, P. P. London dispersion forces in sterically crowded inorganic and organometallic molecules. *Nat. Rev. Chem.* **2017**, *1*, 4.
(35) Ballester, P.; Oliva, A. I.; Costa, A.; Deyà, P. M.; Frontera, A.; Gomila, R. M.; Hunter, C. A. DABCO-Induced self-assembly of a trisporphyrin double-decker cage: thermodynamic characterization and guest recognition. *J. Am. Chem. Soc.* **2006**, *128*, 5560−5569.
(36) Schmittel, M.; He, B.; Fan, J.; Bats, J. W.; Engeser, M.; Schlosser, M.; Deiseroth, H.-J. Cap for copper(I) ions! Metallosupramolecular solid and solution state structures on the basis of the dynamic tetrahedral Cu(phenAr2) $(py)^{2+}$ motif. *Inorg. Chem.* **2009**, *48*, 8192−8200.
(37) Neogi, S.; Schnakenburg, G.; Lorenz, Y.; Engeser, M.; Schmittel, M. Implications of stoichiometry-controlled structural changeover between heteroleptic trigonal Cu(phenAr2) (py)+ and tetragonal Cu(phenAr2) $(py)^{2+}$ motifs for solution and solid-state supramolecular self-assembly. *Inorg. Chem.* **2012**, *51*, 10832−10841.
(38) Schmittel, M.; Mahata, K. A fully dynamic five-component triangle via self-sorting. *Chem. Commun.* **2010**, *46*, 4163−4165.
(39) Mahata, K.; Schmittel, M. From 2-fold completive to integrative self-sorting: a five-component supramolecular trapezoid. *J. Am. Chem. Soc.* **2009**, *131*, 16544−16554.
(40) Schmittel, M.; Mahata, K. Multicomponent assembly of heterometallic isosceles triangles. *Inorg. Chem.* **2009**, *48*, 822−824.
(41) Löffler, S.; Lübben, J.; Wuttke, A.; Mata, R. A.; John, M.; Dittrich, B.; Clever, G. H. Internal dynamics and guest binding of a sterically overcrowded host. *Chem. Sci.* **2016**, *7*, 4676−4684.
(42) Because the surface area varies largely with the changes from ground to transition state, the solvent correction has a drastic influence.
(43) **2a** is little more stable than **2b**, ΔE = 0.2 kJ mol^{-1}.

DOI: 10.1021/acs.inorgchem.7b00740
Inorg. Chem. XXXX, XXX, XXX−XXX